LOAD CAPACITY OF HELICOIL® INSERTS IN ABS-M30 MATERIAL USED FOR ADDITIVE MANUFACTURING

ZBYNEK PASKA[1], JAROSLAV ROJICEK[1], FRANTISEK FOJTIK[1], VACLAV KRYS[2], MARTIN FUSEK[1], DAGMAR LICKOVA[1],

[1]Department of Applied Mechanics, Faculty of Mechanical Engineering, Ostrava-Poruba, Czech Republic

[2]Department of Robotics, Faculty of Mechanical Engineering, Ostrava-Poruba, Czech Republic

DOI: 10.17973/MMSJ.2021_12_2021111

zbynek.paska@vsb.cz

This paper deals with experimental investigations and numerical simulations of HELICOIL® inserts in ABS-M30 plastic. The aim is to explore the possibilities of modelling HELICOIL® inserts using Finite Element Method (FEM) and thus predict the load-bearing capacity of these inserts. The motivation was based on a previously published article that dealt with the topological design of the robot manipulator arm shape. During the mechanical tests, the structure of the arm did not collapse, but the HELICOIL® inserts were torn out. To determine the load-bearing capacity of HELICOIL® inserts, the necessary experimental tests were designed and carried out. FEM calculations of the inserts were adjusted to the obtained data. The results from the FEM were verified in an experimental validation test.

KEYWORDS

HELICOIL® FEM simulation, HELICOIL® experiments, ABS-M30, Additive manufacturing, Cohesive contact.

1 INTRODUCTION

In the previous article [Paska 2020], attention was paid to the design of the shape of the robot manipulator arm (see Figure 1) by means of topological optimization performed in the ANSYS software. Three versions of the robot manipulator arm were presented.

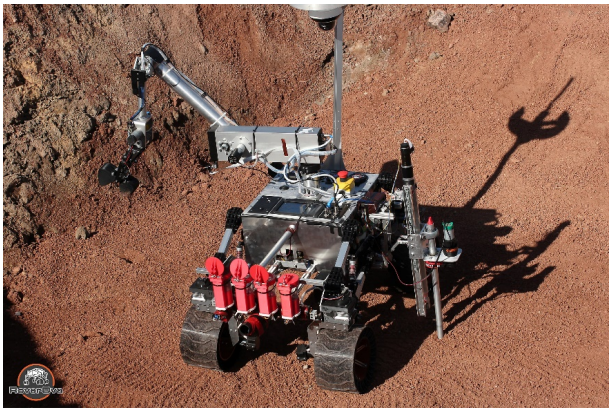

Figure 1. Mobile robot manipulator

ABS-M30 material was chosen to make the final shape of the arm. This material was simulated with a linear elastic material model whose parameters were determined from the data of a simple tensile test and Digital Image Correlation (DIC) measurements. The real behavior of the robotic arm in [Paska 2020] was measured at several typical loads using an accelerometer on the effector. Typical manipulation tasks last 1 to 5 minutes, so the experiments were designed to represent behavior in the range up to 10 minutes. The robot is designed for outdoor use and can be used at different temperatures (e.g. from -20 °C to 40 °C), but depending on the experimental equipment, tests were carried out in the range (from 20 to 80 °C), see [Fusek 2021]. In this work, Anand material model was used to simulate the behavior of ABS-M30 material and loading conditions lasting up to 10 minutes and in the mentioned temperature range, for which the material parameters were determined and validated.

The next step is the experimental testing of the resulting manipulator arms and the comparison with the simulation. The optimized arm shapes are attached to the manipulator with bolts and so-called HELICOIL® inserts.

The aim of the work is to test the behavior of the HELICOIL® inserts in ABS-M30 material. This includes both the experimental and numerical solution, design and execution of experiments and numerical simulations of the HELICOIL® insert itself. The aim is also to explore the possibilities of FEM modeling of the HELICOIL® insert and thus prepare a computational model for the future solution of the entire robot manipulator arm made of 3D printed ABS-M30 material.

2 HELICOIL® INSERTS

The HELICOIL® insert (see Figure 2) is used to repair damaged threads or to increase the load-bearing capacity of a bolt connection. The system is mainly used with aluminum alloys but can be also used with plastics [Boellhoff 2021]. The HELICOIL® inserts are highly wear resistant, corrosion resistant and the surface quality provides low friction in the threads. The insert also causes a better stress distribution in the threads and thus an increase in the load-bearing capacity of the connection. This system is advantageous for connections made of softer materials (e.g. aluminum alloys), where the connection is frequently disassembled, and the thread can be damaged by wear [HELICOIL 2021]. In addition to HELICOIL® inserts, several special inserts are used for plastic materials, which are pressed into the material or inserted directly into the melt.

Figure 2. HELICOIL® inserts [HELICOIL 2021]

There are many publications dealing with the simulation of bolted joints [Kim 2007], [Wang 2021], [Zhang 2020]. However, the number of publications dealing with simulations of bolted joints in the form of modeling all individual threads is much smaller [Lehnhoff 1996]. In the literature [Chen 1999], the author deals with the FEM analysis of individual threads and determines their load (load bearing fraction). The thread friction is included, and the problem is also solved analytically. The axisymmetric solution is only a simplification because it cannot consider the effect of the pitch of the thread. The influence of friction in the thread, the pitch, and for example, the modulus of elasticity on the dependence of tightening torque and preload in

the bolt is investigated in the article [Zhou 2015] (3D model and 3D FEM calculations are used).
In the paper [Meram 2019], the influence of HELICOIL® inserts on the increase of the load-bearing capacity of the bolted joint in carbon fiber polymer (CFRP) was investigated and the results were compared with those obtained from specimens without HELICOIL® inserts. These are purely experimental tests without FEM analysis. The connections were loaded with compressive force and torque. In both loading cases, there was a significant increase in the load-bearing capacity of the connections with HELICOIL® inserts. The load-bearing capacity of the bolted joint in printed polycarbonate (PC-10) is studied in article [Lipina 2016]. From the mentioned publication it is shown that the influence of the specimen orientation during printing and the number of 'contours' (in 3D printing, the term perimeter is used) has a significant influence on the load bearing capacity of the bolt joint. The load capacity is also increased using HELICOIL® inserts. The influence of the alignment of parts in 3D printing on their mechanical properties is investigated in the article [Lipina 2018], which also addresses the issue of bolting parts manufactured with FDM.

3 ANAND MATERIAL MODEL

The Anand material model is used for the simulation and the values of its parameters were taken from the paper [Fusek 2021].
Anand viscoplastic model is already included in most commercial finite element programs. The Anand model is typically used for solder alloys [Cheng 2000], [Motalab 2012], but the authors successfully test it for the material used for 3D printing, ABS-M30 material. Anand viscoplastic model is also applicable to general viscosity problems that include the influence of strain rate and the influence of temperature. The model of Anand is a complex material model that has introduced an internal variable s (deformation resistance), a variable that represents the resistance to the plastic behaviour of the material.
The rate of plastic deformation is described by the following relationship:

$$\dot{\boldsymbol{\varepsilon}}_{\mathrm{pl}} = \dot{\varepsilon}^{\mathrm{a}}{}_{\mathrm{pl}} \left(\frac{3}{2}\frac{\mathbf{S}}{q}\right), \tag{1}$$

where $\dot{\boldsymbol{\varepsilon}}_{\mathrm{pl}}$ is the tensor of the inelastic strain rate and $\dot{\varepsilon}^{\mathrm{a}}{}_{\mathrm{pl}}$ is the rate of accumulated equivalent plastic strain, $\dot{\varepsilon}^{\mathrm{a}}{}_{\mathrm{pl}}$ is given by the equation:

$$\dot{\varepsilon}^{\mathrm{a}}{}_{\mathrm{pl}} = \left(\frac{2}{3}\,\dot{\boldsymbol{\varepsilon}}_{\mathrm{pl}} : \dot{\boldsymbol{\varepsilon}}_{\mathrm{pl}}\right)^{\frac{1}{2}}, \tag{2}$$

where the operator ':' stands for inner product of tensors. $\mathbf{S}$ is the deviator of Cauchy stress tensor, which can be expressed by the following relation:

$$\mathbf{S} = \boldsymbol{\sigma} - p\mathbf{I}, \tag{3}$$

where $\boldsymbol{\sigma}$ is the Cauchy stress tensor, $\mathbf{I}$ represents a second-order unit tensor, $\mathbf{p}$ is defined as one-third of the trace of the tensor matrix $\boldsymbol{\sigma}$, see the following relation:

$$p = \frac{1}{3}\mathrm{tr}(\boldsymbol{\sigma}). \tag{4}$$

The quantity q is the equivalent stress according to the following relation:

$$q = \left(\frac{3}{2}\mathbf{S}:\mathbf{S}\right)^{\frac{1}{2}}. \tag{5}$$

The rate of accumulated plastic deformation depends on q and on the internal state variables s. This dependence can be expressed by the following relation:

$$\dot{\varepsilon}^{\mathrm{a}}{}_{\mathrm{pl}} = \mathrm{A}e^{\left(-\frac{Q}{R\theta}\right)}\left\{\sinh\xi\frac{q}{s}\right\}^{\frac{1}{m}}, \tag{6}$$

where A, ξ and m are the model constants, Q is the activation energy, R is the universal gas constant, θ is the absolute temperature and s is the internal state variable.

The development of the internal state parameter s is described as follows:

$$\dot{s} = \oplus h_o \left|1 - \frac{s}{s^*}\right|^a \dot{\varepsilon}^{\mathrm{a}}{}_{\mathrm{pl}}, \tag{7}$$

where a and h_o are constants, s^* represents the saturated value of the internal parameter. The $\oplus$ operator is defined to return $+1$ if $s \leq s^*$, otherwise return -1. The effect of softening or hardening is included in the model by this operator. The saturation values of s^* depending on the rate of equivalent plastic deformation $\dot{\varepsilon}^{\mathrm{a}}{}_{\mathrm{pl}}$ and can be expressed as follows:

$$s^* = \hat{s}\left\{\frac{\dot{\varepsilon}^{\mathrm{a}}{}_{\mathrm{pl}}}{A}e^{\left(\frac{Q}{R\theta}\right)}\right\}^n, \tag{8}$$

where $\hat{s}$ and n represent constants.

Expression (7) shows that the development of the parameter s depends on the rate of the equivalent plastic deformation and at the same time on the current state of the internal state parameter s.

E_{20} [MPa]	s_0 [MPa]	Q/R [K]	A [1/s]	x_i
1196	18.0	9486	3263	8.82
m [–]	**h_0 [MPa]**	**$\hat{S}$ [MPa]**	**n [–]**	**a [–]**
0.213	138175	43.6	0.0226	3.527

Table 1. Parameters of the Annand material model [Fusek 2021]

Table 1 shows only the result values of Anand material model used for the FEM simulation of the HELICOIL® insert pull-out. E_{20} indicates the modulus of elasticity for the ABS-M30 material at 20 °C.

4 ROBOT MANIPULATOR ARM TESTING

An arm whose shape was designed by topological optimization [Paska 2020] and whose weight was 0.178 kg was subjected to a bending test (see Figure 3).

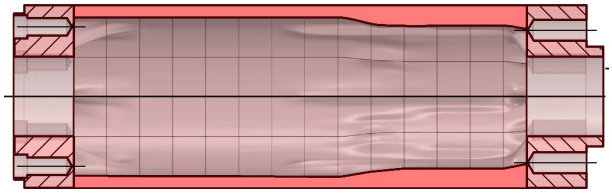

Figure 3. Dimensions of the arm: outer diameter 55 mm and length 178 mm [Paska 2020]

The arm was fixed with a specially designed fixture. The fixture consists of aluminium structural profiles and a custom-made steel plate on which a printed arm is fixed with an M5 bolts. The structure can be seen in Figure 4 and on Figure 5.

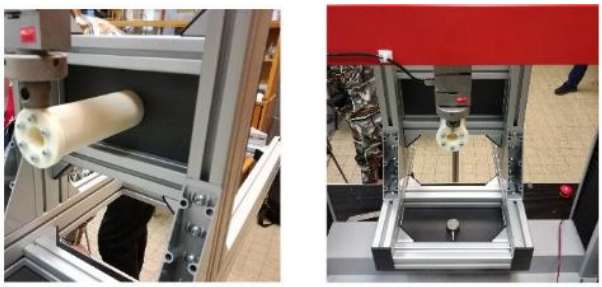

Figure 4. Bending test of the arm

The designed device allows testing arms of different sizes. The picture of the device and its basic parameters are shown in Figure 5.

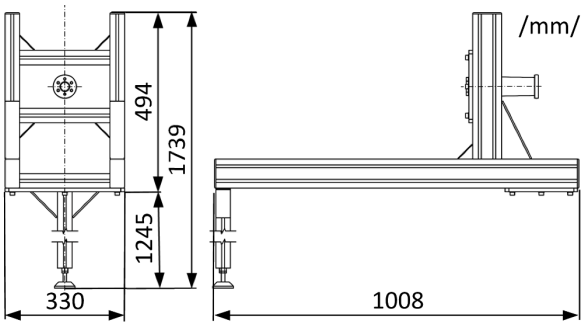

Figure 5. Schematic diagram of the fastening device

The bending test was controlled by deformation. The type of loading can be seen in Figure 6. The measured response is then visible in Figure 7. The loading rate was 1 mm/min and can therefore be considered as a quasi-static test in terms of strain rate.

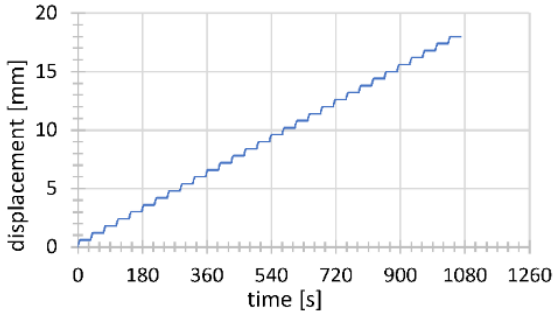

Figure 6. Load test settings

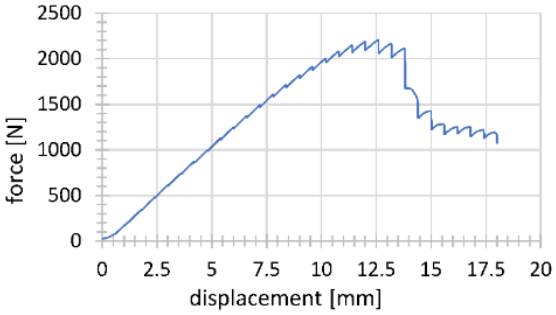

Figure 7. Dependence of the force on the displacement

The load did not cause the arm structure to collapse, but the HELICOIL® inserts were gradually pulled out of the arm flange, as shown in Figure 8. To simulate the behaviour of the inserts in terms of load capacity, a series of tests had to be performed. These tests are described in more detail in the following chapter.

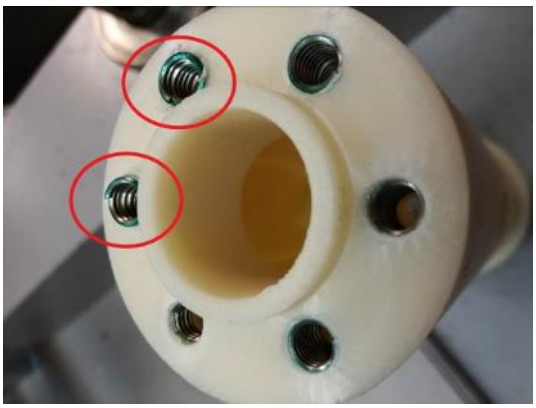

Figure 8. HELICOIL® inserts torn out from the arm flange

The optimized arm structure is therefore not fully utilized in terms of strength and the entire optimization process is not useful. For this reason, it was decided to investigate the load bearing capacity of HELICOIL® inserts in the printed material using the proposed experiments and FEM analyses.

5 TESTING OF HELICOIL® INSERTS

A total of 18 samples were printed from ABS-M30 material, which were then equipped with a HELICOIL® insert for M5 bolts. Six different configurations (H1, H2, H3, V1, V2 and V3) were printed, three samples each. The designation **H**, or **V** indicates the **H**orizontal, or **V**ertical orientation of the hole of the sample in the printing process. The numbers 1, 2, 3 indicate the number of 'contours' layers during printing. On Figure 9(a) is a schematic representation of the model with HELICOIL® insert, Figure 9(b) shows the position of the thread insert in the specimen. The average length of the HELICOIL® insert was 7 mm and consisted of 9 threads.

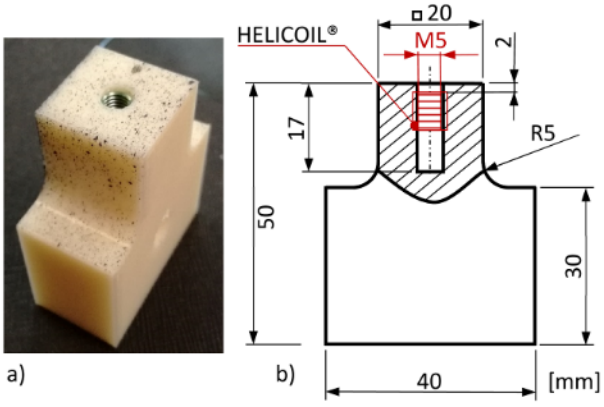

Figure 9. (a) the sample was provided with a contrast pattern for DIC measurements; (b) specimen dimensions

The specimens were placed into a Testometric M500-50CT testing machine **[Testometric 2021]** as shown in Figure 10. The camera used for the DIC measurements can be seen in the figure. The M5 bolt was also fitted with a contrasting pattern. The bolt was screwed into the moving crosshead of the tearing machine through a conical insert. Thanks to the conical insert, the possible small offset of the HELICOIL® insert and the M5 bolt has been eliminated. DIC measurements were used to record the position of the point on the M5 bolt and the point near the top of the sample. Using the DIC measurements, the exact value of the displacement of the bolt (and thus of the HELICOIL® insert itself) relative to the specimen could be determined.

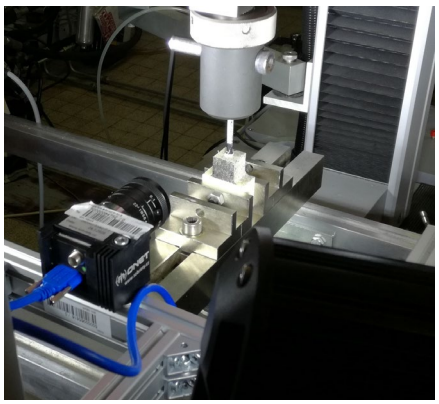

Figure 10. Clamping the specimen in a testing machine and measuring with DIC

Mercury RT® system from Sobriety s.r.o. was used for DIC measurements with one camera (1x5MPx@60 fps, max 400 fps). The force parameters were determined by a force sensor (measuring range 50 kN and measuring accuracy ± 10 N), which is part of the testing machine. All measured signal quantities were time synchronized with each other.

5.1 Experiments setup

One specimen from each set (H1/2/3; V1/2/3) was loaded by a simple tensile test at a constant speed of 2 mm/min, except for the first specimen from set H1, where the loading speed was 5 mm/min. The HELICOIL® insert is loaded until it is completely pulled out. The test set in this way is referred as 'experiment 1'. One specimen from each set was loaded with a tensile test at a speed of 2 mm/min with a time delay of 5 min ('experiment 2'), the experimental procedure is shown in Figure 11. One specimen from each set was loaded with a graded tensile test at a speed of 2 mm/min with a time delay 60 s and a deformation step of 0.25 mm ('experiment 3'), see Figure 12.

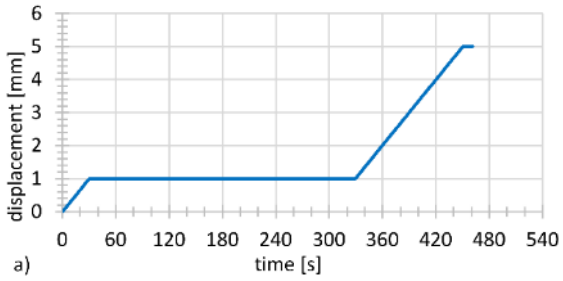

Figure 11. Setup of 'experiment 2'

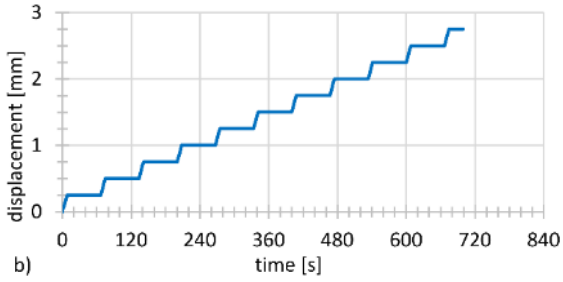

Figure 12. Setup of 'experiment 3'

5.2 Measured load capacity of the HELICOIL® insert

The patterns are labelled alphanumerically. The letter of the alphabet refers to the orientation of the pattern (axis of the hole for the HELICOIL® insert) in 3D printing (**H**orizontal and **V**ertical orientation). The numerical value after the letter refers to the number of contour layers (perimeter). The aim of this chapter will be to clarify the influence of these two factors on the load capacity of the HELICOIL® insert.

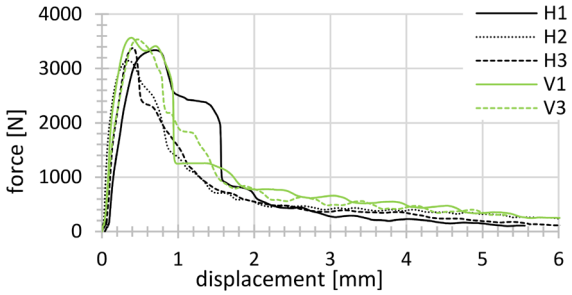

Figure 13. Force dependence on the displacement of the HELICOIL® insert ('experiment 1').

The course of the force as a function of the pull-out value of the HELICOIL® insert for the first test is shown in Figure 13. It can be seen from the figure that the maximum force value is approximately the same for all specimens. To accurately determine the influence of specimen orientation and the number of contour layers on the load capacity of the insert, more detailed statistical evaluation on many specimens would be required. However, in this article, the focus has been primarily on the HELICOIL® insert simulation rather than statistical processing, which could be the next step.

The force-time dependence for 'experiment 2' can be seen in Figure 14. These experiments partially capture the effect of force relaxation. The second number of the specimen designation in the graph legend in Figure 14 indicates the value of the displacement of the HELICOIL® insert, which corresponds to the maximum value of the force in the left part of the graph. As an example, we give the designation V3_0.24, where at a force value of 3413 N the displacement of the HELICOIL® insert was 0.24 mm. The test was set so that the displacement of the crosshead corresponds to a value of 1 mm (see Figure 11), but due to the stiffness of the fastening and the inherent elasticity of the specimen, the actual value of the displacement of the insert is smaller. Therefore, it can be seen from Figure 14 that in this experiment it is not possible (due to a different value of the HELICOIL® insert displacement and thus a different load) to determine the degree of influence of the specimen orientation during 3D printing and the number of perimeters on the load capacity.

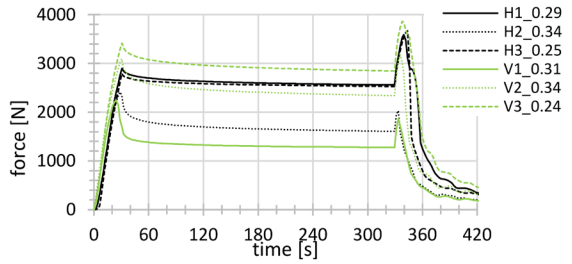

Figure 14. The magnitude of the force as a function of time for 'experiment 2'.

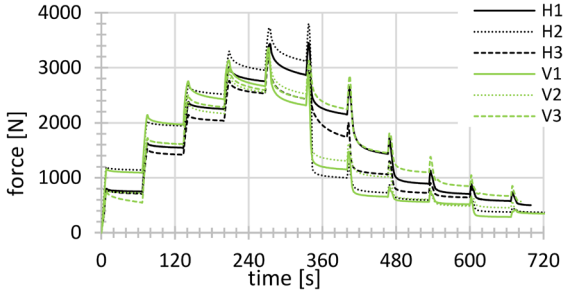

Figure 15. The magnitude of the force for 'experiment 3'

The response for 'experiment 3' is shown in Figure 15. The configuration of this experiment also allows us to partially capture the effect of force relaxation at different values of the loads acting on the HELICOIL® insert. Significant differences between specimens can be seen in the figure, but these differences cannot be generalized to determine which specimen orientation is the best or worst in terms of load capacity.

6 FEM ANALYSIS OF HELICOIL® INSERTS

The FEM analyses were performed in MSC.Mark software, which is suitable for nonlinear tasks [Marc 2021]. The data from experiment H1 are shown in Figure 16 in force-time and displacement-time coordinates, where displacement represents the applied load and force represents the expected response on the bolt. It is not necessary to tune the FEM simulation to the entire curve of the experiment, therefore, the simulation is performed only up to a time of about 16 s, when the HELICOIL® insert was torn out.

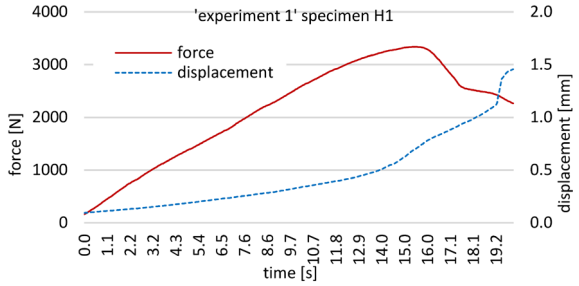

Figure 16. Dependence of force on time and displacement on time for experiment H1, which was used to set up the FEM calculation

In the literature we did not find any data for FEM simulations of HELICOIL® inserts. Therefore, several variants of simulation of this type of connection were designed and tested:

1. Detailed modelling of threads and contact in 3D, see e.g. [Chen 1999]. It was very computationally and time consuming and therefore difficult to apply to a real task with an arm (see Figure 4 and Figure 8).
2. Model with axis symmetry. Difficult to apply to a real arm task.
3. Model replacing the real complex HELICOIL® insert behaviour by a bonded type of contact, see [Marc 2018]. This approach is applicable to a real task and is described in more detail below.

All variants were tested in an experiment called H1, where the bolt is loaded with a continuously increasing displacement until it is torn out.

For the simulation, a model of the upper part of the specimen was created - using a rectangle 20x20 mm with a height of 20 mm with a hole with a diameter of 5 mm, the behaviour of the material was simulated using Anand material model. The bolt was modelled as a cylinder with a diameter of 5 mm and a length of 40 mm. The length of the threaded part, which transmits the load to the specimen is 7 mm (corresponding to the length of the HELICOIL® insert). The bolt material was simulated by linear elastic behaviour (steel modulus of elasticity E = 210000 MPa, Poisson ratio μ = 0.3). To simplify the simulation, two symmetry planes were used (Sym 1 and Sym 2). A four-node element was used to create the mesh, and the resulting model contains 5054 nodes and 22653 elements. The resulting model is shown in Figure 17. The bottom of the sample was fixed, and the top of the bolt was loaded by displacement.

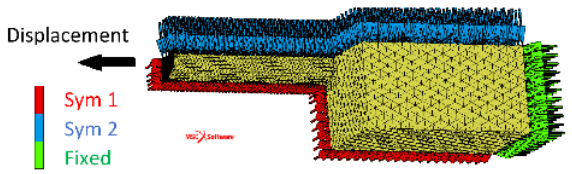

Figure 17. Geometry and boundary conditions

	displ.	stress		displ.	stress
p1	0	0	p6	0.05	23
p2	0.0001	5	p7	0.1	23
p3	0.0005	10	p8	0.2	20
p4	0.002	15	p9	0.5	15
p5	0.01	20	p10	1	15

Table 2. The values of the parameters (p1-p10) for setting up the contact

A simple bonded contact provides acceptable results only up to 2000 N, see Figure 18. The behaviour of the bonded contact type in MSC.Marc can be modified by a so-called cohesive contact. Cohesive contact can be defined, for example, by the stiffness given by the value of the contact stress as a function of the displacement, which was used in this case. The displacement is the relative displacement between the contacting and contacted point along the contact shear (Table 2) or normal (Table 3) direction. The cohesive contact is therefore entered using two tables for the normal and shear directions of the load on the HELICOIL® insert, which can be used to modify the behaviour of the contact. The tables were determined by trial-and-error method. It is possible to capture the behaviour of the HELICOIL® inserts very well throughout the analysed time interval (16 s), see Figure 18.

	p11	p12	p13	p14	p15	p16	p17
displ.	0	0.0005	0.015	0.03	0.1	0.5	1
stress	0	8	10	10	8	7	6

Table 3. The values of the parameters (p11-p17) for setting up the contact normal

Figure 18 shows the force-time curve for experiment H1 in a simple tensile test setup ('experiment 1') and a comparison with the results from the FEM simulation. Here are the results for the simply bonded contact and for the cohesive contact. Cohesive contact gave the best results in the whole examined interval.

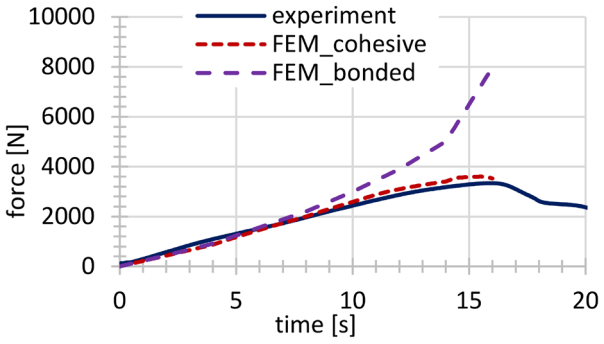

Figure 18. Comparison of the simple tensile test 'experiment 1' for specimen H1 with FEM simulations using bonded contact and cohesive contact

Figure 19 shows the distribution of the HMH equivalent stress distribution at times 14 and 16 s.

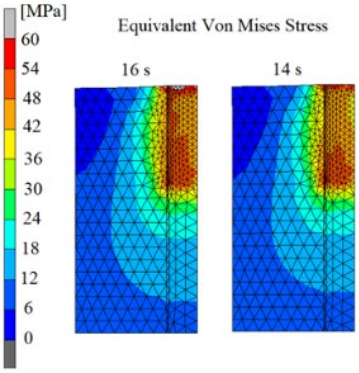

Figure 19. Example of HMH stress distribution at the moment when the HELICOIL® insert starts to be pulled out (the insert is moving upwards)

However, these stress distributions obtained by FEM analysis cannot be validated experimentally. The DIC data on the sample surface is too far from the contact and the values of the forces and displacements were used to estimate the stiffness of the cohesive contact, therefore for validation, the data from the 'experiment 3' are used, see Figure 20. In the first two stages the curves agree very well, while in the others the behaviour is different. In this test, the viscous component is more pronounced, which is not very noticeable in the classical tensile load.

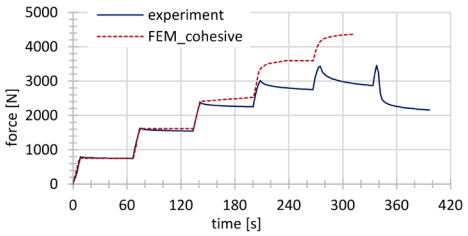

Figure 20. Comparison of 'experiment 3' for sample H1 with FEM simulation of the cohesive contact

The results show that the cohesive contact set by the Table 2 and Table 3 can be used for simulating the behaviour of HELICOIL® inserts even for more complex arm simulations (see Figure 20). However, only for a simple, linearly increasing load of the arm, where the load corresponds to the ordinary extraction of the HELICOIL® insert when the viscous component has only a minimal influence.

7 DISCUSSION

From our point of view, it is necessary to predict the load capacity of the HELICOIL® insert in the form of numerical FEM calculations. The numerical calculations were performed in the MSC.Mark software. The aim was to match the calculation on the selected experiment (Figure 16) and to test the prediction on the validation experiment (Figure 20). Several variants of the calculation were tried, including the possibility of modelling the entire threaded insert in the form of a bolted joint in all its shape complexity, but the results were not good. The approach of modelling the HELICOIL® insert with a cohesive contact worked best and provided acceptable results.

From the previous chapters it is evident that:

- The connection method used with HELICOIL® inserts is the weakest element of the arm, see Figure 8.
- The expected arm load [Paska 2020] is very low (up to 50 N) and is significantly lower than the measured value, see Figure 7 (approx. 2000 N). The designed arm, including the attachment, is therefore sufficiently dimensioned.
- In [Paska 2020], 3 arm variants were designed by means of topological optimization. In this contribution intermediate variant was used with a safety factor of 5 maximum reduced stress compared to the assumed yield strength of ABS-M30 (10 MPa). From the tensile test published in [Paska 2020], it can be estimated that the ultimate strength is about three times the yield strength. This partly explains the difference between the assumed arm load and the load measured when the HELICOIL® inserts were pulled out.
- For short loading times (up to 10 minutes), the material model can be replaced by a linear elastic material model and insert by a fixed boundary condition. The load of HELICOIL® inserts of a certain size depends on the specimen configuration, see Figure 15. For the variant simulated by FEM, the force per 1 HELICOIL® insert up to 2000 N can be recommended (see Figure 18 and Figure 20).

The proposed method of experimental testing of HELICOIL® inserts and their simulation with cohesive contact, even for complex models, provides useful results and will be further developed.

To determine the parameters of the cohesive contact, we plan to use the FEMU approach in the future, which is used, for example, in [Fusek 2021] to identify material parameters. This method allows the use of more experiments to identify parameters, including graded tensile tests. From the point of view of the practical use of the given material and HELICOIL® inserts, it would be useful to extend the experimental and numerical investigations to the fatigue field.

We will deal with the issue of FEM solution of the robot manipulator arm equipped with HELICOIL® inserts in more detail in the next article. The reason for this is the fact that the model of the arm was made a long time ago and from a different series of ABS-M30 material than the samples with a HELICOIL® insert. In our experience, the material parameters for 3D printing materials can change significantly, which can be caused by several factors. These factors include for example: the production series of the material for 3D printing; the settings of the 3D printer; the aging of the material; moisture absorption by the material; the storage of the material.

8 CONCLUSIONS

The article was focused on measuring the load capacity of HELICOIL® inserts. The motivation for this research was based on the conducted experiment of the robot manipulator arm, which was created based on topological optimization and described in the paper [Paska 2020]. In this experiment, the HELICOIL® inserts were torn out and the optimised arm did not collapsed. For this reason, it was necessary to investigate the load bearing capacity of the HELICOIL® inserts in more detail. Eighteen specimens were produced, which were equipped with a HELICOIL® insert. The specimens were made in 6 different configurations of 3D printing and a number of contour layers (perimeters). They were then tested in 3 configurations (settings) of the testing machine. The dependence of the force on the displacement of the HELICOIL® insert was measured using the DIC method. All experimental results are presented in this article.

From the conducted experiments, it is evident that there is no unique configuration of 3D printing that would lead to higher load capacity of the HELICOIL® insert in case of ABS-M30 material. It is not possible to say which position of the specimen

in the printing chamber and how many perimeters are best with regard to the strength of the HELICOIL® insert. To make a reliable statement, a much larger number of tests would have to be performed and statistically evaluated.

Based on Figure 20, it is recommended to use the given HELICOIL® insert up to a force of about 2000 N (this applies to M5 HELICOIL® insert with a length of 7 mm in ABS-M30 material) and then the HELICOIL® insert can be replaced by a fixed connection of the bolt and the flange. At higher strength values, the viscous behaviour starts to become more apparent. The test duration was limited to about 300 s until the HELICOIL® insert was pulled out. When the arm is subjected to a real working condition, more complex stress on the HELICOIL® insert is expected (object handling). These conditions include repeated fatigue loads at longer time intervals. The behaviour and load capacity of the HELICOIL® insert must be considered during design and topology optimization.

About the facts mentioned in the discussion, we always recommend producing test specimens at the same time as manufacturing the functional component for a possible check of the material properties and material parameters. Our experience has shown that the material properties can vary greatly depending on many factors. It is therefore advisable to make the test samples at the same time as the real component.

ACKNOWLEDGMENTS

This article was elaborated under support of the Research Center of Advanced Mechatronic Systems, reg. no. CZ.02.1.01/0.0/0.0/16_019/0000867, within the framework of the Operational Program for Research, Development, and Education.

REFERENCES

[Boellhoff 2021] Wilhelm Boellhoff GmbH & Co.. For high-strength fastenings. Boellhoff, 2021, location [online]. [cit. 25.6.2021] Available from <https://www.boellhoff.com/de-en/products-and-services/special-fasteners/thread-inserts-helicoil.php >.

[Chen 1999] Chen, J.J. and Snih, Y.S. A study of the helical effect on the thread connection by three dimensional finite element analysis. Nuclear Engineering and Design. July 1999, Vol.191(2), pp 109-116. ISSN 00295493. doi:10.1016/S0029-5493(99)00134-X.

[Cheng 2000] Chen, Z.N. et al. Viscoplastic Anand model for solder alloys and its application. Soldering & Surface Mount Technology. August 2000, Vol.12(2), pp 31-36. ISSN 0954-0911. doi:10.1108/09540910010331428

[Fusek 2021] Fusek, M. and Paska, Z. Parameters Identification of the Anand Material Model for 3D Printed Structures. Materials. January 2021, Vol.14, No.3. <https://doi.org/10.3390/ma14030587>.

[HELICOIL 2021] HELICOIL® PLUS. System HELICOIL® Plus, 2021, [online]. [cit. 25.6.2021] Available from < https://www.helicoil.cz/cs/system-helicoil-plus/a-1/ >. (in Czech language).

[Kim 2007] Kim, J., Yoon, J.-Ch., Kang, B.-S. Finite element analysis and modeling of structure with bolted joints. Applied Mathematical Modelling. 2007, 31(5), 895-911. ISSN 0307904X. doi:10.1016/j.apm.2006.03.020.

[Lehnhoff 1996] Lehnhoff, T.F. and Wistehuff, W.E. Nonlinear Effects on the Stresses and Deformations of Bolted Joints. Journal of Pressure Vessel Technology. February 1996, Vol.118(1), pp 54-58. doi:10.1115/1.2842163.

[Lipina 2016] Lipina, J., Krys, V. APPLICATION OF RAPID PROTOTYPING TECHNOLOGY IN DESIGNING ROBOTS AND PERIPHERAL DEVICES. MM Science Journal. 2016, 2016(01), 856-861. ISSN 18031269. doi:10.17973/MMSJ.2016_03_201544.

[Lipina 2018] Lipina, J., Krys, V., Fojtik, F. Tensile Test on Samples Produced by Rapid Prototyping Technology with a Higher Number of Contours. 2018 IEEE 22nd International Conference on Intelligent Engineering Systems (INES). IEEE, 2018, ISBN 978-1-5386-1122-7. doi:10.1109/INES.2018.8523963.

[Marc 2021] HEXAGON MSC Software. Marc Advanced Nonlinear Simulation Solution, 2021, [online]. [cit. 30.6.2021] Available on https://www.mscsoftware.com/product/marc

[Marc 2018] Marc® 2018.1: Volume A: Theory and User Information. Newport Beach, CA 92660, 2018.

[Meram 2019] Meram, A. and Can, A. Experimental investigation of screwed joints capabilities for the CFRP composite laminates. Composites Part B: Engineering. November 2019, Vol.176. ISSN 13598368. doi:10.1016/j.compositesb.2019.107142.

[Motalab 2012] Motalab, M. et al. Determination of Anand constants for SAC solders using stress-strain or creep data. 13th InterSociety Conference on Thermal and Thermomechanical Phenomena in Electronic Systems. July 2012. pp. 910-922. ISBN 978-1-4244-9532-0. doi:10.1109/ITHERM.2012.6231522.

[Paska 2020] Paska, Z. and Rojicek, J. Methodology of arm design for mobile robot manipulator using topological optimization. MM Science Journal. June 2020, pp 3918-3925. ISSN 18031269.

[Testometric 2021] Testometric Co. Ltd. Testometric materials testing machines. 50KN MACHINES, 2021, [online]. [cit. 23.7.2021]. Available from < http://www.testometric.co.uk/50kn/>

[Wang 2021] Wang, P., You, Y., Xu, Q., Wang, Q., Liu, F. Shear Behavior of Lapped Connections Bolted by thread-fixed one-side bolts at elevated temperatures. Fire Safety Journal. 2021, 125. ISSN 03797112. doi:10.1016/j.firesaf.2021.103415.

[Zhang 2020] Zhang, D., Wang, G., Huang, F., Zhang, K. Load-transferring mechanism and calculation theory along engaged threads of high-strength bolts under axial tension. Journal of Constructional Steel Research. 2020, 172. ISSN 0143974X. doi:10.1016/j.jcsr.2020.106153.

[Zhou 2015] Zhou, Y.Q.H. and Wang, L. Finite element analysis of relationship between tightening torque and initial load of bolted connections. Advances in Mechanical Engineering. May 2015, Vol.7(5), pp 54-58. ISSN 1687-8140. doi:10.1177/1687814015588477

CONTACTS:

Ing. Zbynek Paska
Department of Applied Mechanics
VSB – Technical University of Ostrava
Faculty of Mechanical Engineering
17. listopadu 15
708 33 Ostrava – Poruba,
Czech Republic
e-mail zbynek.paska@vsb.cz